Enhanced Group-Based Chirp Spread Spectrum Modulation: Design and Performance Analysis

Quantao Yu, Hua Wang, *Member, IEEE*, Dongxuan He, and Zhiping Lu

***Abstract*—LoRa is one of the most prominent low power wide area network (LPWAN) technologies for Internet of Things (IoT) applications. As the core technique of LoRa physical (PHY) layer, chirp spread spectrum (CSS) modulation is employed to support low power and long range communications. Although it provides a compelling trade-off between coverage and data rate, the relatively low spectral efficiency (SE) is still a limiting factor for its extensive applications. In this paper, we propose two enhanced group-based CSS modulation schemes, named IQ-GCSS (in-phase and quadrature group-based CSS) and TDM-GCSS (time domain multiplexed group-based CSS), which can achieve much higher SE than the conventional LoRa modulation. The transmitter architectures of our proposed modulation schemes are presented along with both coherent and non-coherent detection methods. Moreover, an overall performance analysis of our proposed schemes is provided in terms of bit error rate (BER) and computational complexity. Numerical results not only validate the accuracy of our theoretical analysis but also demonstrate substantial performance improvements of our proposed schemes in terms of effective throughput compared to the classical counterparts.**

***Index Terms*—IoT, LPWAN, LoRa, chirp spread spectrum, performance analysis.**

I. Introduction

THE ever-increasing demand for the Internet of Things (IoT) puts forward new requirements for wireless technologies. In particular, a multitude of IoT applications, such as smart city, precision agriculture, asset tracking, and environmental monitoring, require low power and long range communications, which has driven the emergence and proliferation of low power wide area network (LPWAN) [1]. Among the state-of-the-art LPWAN technologies, LoRa has attracted widespread interest from both academia and industry [2].

From the technical point of view, LoRa can be categorized into two layers: physical (PHY) layer using chirp spread spectrum (CSS) modulation (i.e., LoRa modulation) and medium access control (MAC) layer with ALOHA-based protocol (i.e., LoRaWAN protocol). Although it is a proprietary technology patented by Semtech Corporation, several studies have provided a detailed mathematical description of LoRa modulation. For example, Vangelista [3] first gave a digital signal processing description of LoRa modulation and provided a theoretical derivation of the optimum receiver based on discrete Fourier transform (DFT). Moreover, in order to give a more rigorous description of LoRa modulation, the authors in [4] provided a complete characterization of LoRa signal model, including its analytical expressions in the time domain as well as closed-form expressions of continuous and discrete spectra.

Based on the mathematical descriptions of LoRa modulation, the authors in [5] provided its closed-form approximations for the underlying bit error rate (BER) performance in both additive white gaussian noise (AWGN) and Rayleigh fading channels. In general, due to the processing gain of LoRa modulation, the transmitted information can be recovered even when the received signal-to-noise ratio (SNR) is negative, indicating its high energy efficiency (EE) for satisfying the low power and long range communication requirements of various IoT applications. However, the high EE of LoRa modulation is achieved at the cost of low SE, which has become a bottleneck for its extensive applications [2], [6], [7]. Therefore, some researchers have proposed alternative CSS-based modulation schemes to improve the SE and data rate, which can be collectively referred to as LoRa-like modulation schemes.

A. Related Works

Based on the number of chirps in one message symbol, the authors in [8] proposed to classify the existing LoRa-like modulation schemes into three categories: (i) single chirp, (ii) multiple chirps, and (iii) multiple chirps with index modulation. From the implementation perspective, we present a more specific classification according to the design techniques used in these LoRa-like modulation schemes.

1) Multi-Parameter CSS Modulation: Since the conventional LoRa modulation only encodes information bits in the initial frequency shifts of the modulated upchirps, one feasible way to tackle this low-data-rate issue is to encode additional information bits by exploiting other chirp signal parameters, which can be characterized as *multi-parameter CSS modulation*. In general, for a transmitted chirp, there are four different parameters that can be utilized to encode the information bits, i.e., amplitude, chirp rate, initial frequency shift, and initial phase shift. Nguyen *et al.* [9] and Bomfin *et al.* [10] proposed to embed extra information bits in the initial phase shifts of the modulated upchirps, giving rise

This work was supported by the State Key Laboratory of Wireless Mobile Communications, China Academy of Telecommunications Technology under Grant CATT.KX.2023.161; in part by the National Key Research and Development Program of China under Grant 2020YFB1807900; in part by the National Natural Science Foundation of China under Grant 62101306; and in part by the BIT Research and Innovation Promoting Project under Grant 2023YCXY029. *(Corresponding authors: Hua Wang; Dongxuan He.)*

Q. Yu, H. Wang, and D. He are with Beijing Institute of Technology, Beijing 100081, China(e-mails: 3120215432@bit.edu.cn; wanghua@bit.edu.cn; dongxuan_he@bit.edu.cn).

Z. Lu is with Beijing University of Posts and Telecommunications, Beijing 100876, China(e-mail: luzp@cict.com). Z. Lu is also with China Academy of Telecommunications Technology (CATT), Beijing 100191, China.

TABLE I
CLASSIFICATION OF STATE-OF-THE-ART LORA-LIKE MODULATION SCHEMES

Category	Modulation Schemes
Multi-Parameter CSS Modulation	PSK-LoRa [9], [10], E-LoRa [11], DCRK-CSS [12], SSK PSK-LoRa [13]
Signal Set Extension	ICS-LoRa [14], SSK-LoRa [15], EICS-LoRa [16], SSK ICS-LoRa [17]
Chirp Multiplexing	IQ-CSS [18], TDM-LoRa [19], DO-LoRa [20], GCSS [21]
Index Modulation	IM-CSM [22], FSCSS-IM [23], FBI-LoRa [24]
Hybrid CSS Modulation	ePSK-LoRa [25], DM-CSS [26], DPSK-MM-CSS [27], IQ-CIM [28]

to PSK-LoRa (phase shift keying LoRa) modulation. The so called E-LoRa (extended LoRa) modulation can be viewed as a special variant of BPSK-LoRa modulation [11]. Besides, encoding additional information bits in the chirp rate has been proposed in [12], named discrete chirp rate keying CSS (DCRK-CSS) modulation. Recently, slope-shift-keying PSK-LoRa (SSK PSK-LoRa) modulation has also been proposed in [13], which exploits the combination of chirp rate, initial frequency shift, and initial phase shift to convey the information bits.

2) Signal Set Extension: Another approach to improve the SE of LoRa modulation is to introduce new available signal set based on the original upchirps. The most representative schemes are interleaved-chirp-spreading LoRa (ICS-LoRa) modulation [14] and SSK-LoRa modulation [15]. In ICS-LoRa, interleaved versions of the original upchirps constitute a new signal set, which can add one more information bit within each message symbol. Similarly, apart from the original upchirps, SSK-LoRa uses downchirps as the newly introduced signal set to convey one additional information bit within each symbol.[1] Besides, enhanced schemes have also been proposed in [16] and [17], called EICS-LoRa (enhanced ICS-LoRa) and SSK ICS-LoRa, respectively. More specifically, multiple different interleavers are used in EICS-LoRa to generate different interleaved versions of the original upchirps, thus further increasing the SE and data rate. SSK ICS-LoRa uses upchirps, downchirps, interleaved upchirps, and interleaved downchirps simultaneously, which can carry two more information bits per symbol compared to the conventional LoRa modulation.

3) Chirp Multiplexing: Although the above mentioned modulation schemes are more spectral efficient than the conventional LoRa modulation, the SE improvement is still marginal since only one or two extra information bits are added within each message symbol in most cases. Therefore, several recent studies focus on increasing the SE more significantly, the core idea of which is *chirp multiplexing*. For example, the authors in [18] proposed IQ-CSS (in-phase and quadrature CSS) modulation by encoding the information bits in both in-phase and quadrature components of the transmitted signal, which can double the SE of the conventional LoRa modulation. In addition, similar method called TDM-LoRa (time domain multiplexed LoRa) has been proposed in [19], which can double the SE of LoRa modulation at the cost of a marginal BER degradation. Besides, Vangelista *et al.* [20] proposed a LoRa-compatible modulation scheme called DO-LoRa (Dual Orthogonal LoRa) which can also double the SE of LoRa modulation approximately. Moreover, the authors in [21] proposed GCSS (group-based CSS) modulation by introducing a new configurable parameter called group number (GN) into the LoRa PHY layer.

4) Index Modulation: Index modulation (IM) utilizes the indices of certain transmission entities to convey additional information bits. The transmission entities can be either practical or virtual, such as transmit antennas, subcarriers, modulation types, time slots, spreading codes, signal powers and so on. With respect to CSS-based communication systems, the authors in [22] proposed to utilize the indices of spreading factors to convey additional information bits. Additionally, Hanif and Nguyen [23] proposed a frequency-shift CSS system with IM (FSCSS-IM) which can achieve much higher SE than the conventional LoRa modulation by using the index combinations of orthogonal upchirps for message representation. Moreover, the authors in [24] proposed two novel frequency-bin-index LoRa (FBI-LoRa) modulation schemes which can significantly increase the transmission throughput at the expense of a slight BER performance loss.

5) Hybrid CSS Modulation: Some recently proposed LoRa-like modulation schemes can be characterized as *hybrid CSS modulation*, the essence of which is to efficiently combine the above mentioned techniques to further improve the SE and data rate. For example, the authors in [25] proposed an enhanced PSK-LoRa (ePSK-LoRa) modulation by dividing the available bandwidth into multiple sub-bands and introducing different phase shifts to them, which can be viewed as a combination of *multi-parameter CSS modulation* and *chirp multiplexing*. DM-CSS (dual-mode CSS) proposed in [26] can be regarded as an integration of *multi-parameter CSS modulation*, *signal set extension*, and *chirp multiplexing* by: (i) multiplexing even and odd chirps; (ii) using phase shifts of

[1]Note that SSK-LoRa modulation can also be regarded as a kind of DCRK-CSS modulation with two available chirp rates.

0 and π for both even and odd chirps; (iii) utilizing either upchirps or downchirps. Moreover, differential PSK-aided multi-mode CSS (DPSK-MM-CSS) modulation proposed in [27] can also be designed by an integration of *multi-parameter CSS modulation* and *chirp multiplexing* where not only the initial frequency shifts of multiple multiplexed chirps but also the DPSK symbols are utilized to convey the information bits. Besides, IQ-CIM (in-phase and quadrature chirp index modulation) is a straightforward combination of *chirp multiplexing* and *index modulation* [28].

B. Motivation, Contributions and Contents

Against the above background, this paper focuses on the design of new CSS-based modulation schemes to accommodate the ever-increasing transmission demands of heterogeneous IoT applications. Specifically, on the basis of our presented classification, we propose two enhanced GCSS modulation schemes through IQ multiplexing and time domain multiplexing, respectively, named IQ-GCSS modulation and TDM-GCSS modulation, both of which belong to the category of *chirp multiplexing*. Notably, one of the most relevant works in the literature is [29], which proposed to use multiple layers with different positive chirp rates to improve the SE and contributed to a layered CSS (LCSS) modulation. However, only upchirps with varying chirp rates are utilized in LCSS modulation while both upchirps and downchirps are utilized in our proposed TDM-GCSS modulation. More importantly, our work mainly focuses on a grouped signal structure for CSS-based modulation schemes, which is different from [29]. Meanwhile, IQ multiplexing is also well exploited to enhance the SE of the classical counterparts.[2] The main contributions of this paper are summarized as follows.

1) We present a new classification of CSS-based LoRa-like modulation schemes according to their specific design techniques. In particular, state-of-the-art LoRa-like modulation schemes can be classified into five categories, namely, multi-parameter CSS modulation, signal set extension, chirp multiplexing, index modulation, and hybrid CSS modulation, which can provide valuable reference for the design of new CSS-based modulation schemes. For the sake of clarity, classification of the aforementioned LoRa-like modulation schemes is summarized in Table I.
2) We propose two enhanced GCSS modulation schemes, namely IQ-GCSS modulation and TDM-GCSS modulation, which can further enhance the SE and data rate compared to the classical counterparts. More precisely, IQ-GCSS modulation exploits both in-phase and quadrature components of the transmitted signal while TDM-GCSS modulation leverages the modulated upchirps and modulated downchirps simultaneously. Moreover, the transmitter architectures of our proposed modulation schemes are presented along with both coherent and non-coherent detection methods.
3) We provide an overall performance analysis of our proposed modulation schemes in terms of BER and demodulation complexity. Specifically, approximate closed-form expressions for BER performance of both IQ-GCSS modulation and TDM-GCSS modulation are obtained over both AWGN and Rayleigh fading channels. Moreover, the computational complexities of symbol detection are analyzed. Numerical results not only verify the accuracy of our theoretical analysis but also demonstrate substantial performance improvements of our proposed schemes in terms of effective throughput.

[2]It's very interesting for future works to combine the layered and grouped signal structure, as well as IQ multiplexing to further enhance the SE.

The remainder of this paper is organized as follows. Firstly, Section II presents the fundamentals of LoRa modulation and GCSS modulation. Section III demonstrates the system model of our proposed IQ-GCSS modulation and TDM-GCSS modulation, including their tranmission and detection. Moreover, an overall performance analysis of our proposed modulation schemes is provided in Section IV. Numerical results and discussions are presented in Section V. Finally, Section VI concludes the whole paper.

II. Preliminaries

A. Basic Definitions

The basic definitions of some main notations throughout this paper are presented here.

- B is the occupied bandwidth of radio signals, which is typically set to be 125 kHz, 250 kHz, or 500 kHz.
- SF is the spreading factor of LoRa modulation ranging from 7 to 12, which determines the processing gain and denotes the number of information bits within each LoRa symbol.
- GN is a configurable parameter called the number of groups introduced in GCSS modulation.
- T is the number of information bits carried by each independent group in GCSS modulation.
- S is the total number of information bits carried by GN groups in GCSS modulation.

In the complex baseband-equivalent form, each chirp can be defined by $M = 2^{SF}$ samples. We denote the basic upchirp and basic downchirp as $u[n]$ and $d[n]$, respectively, expressed as

$$u[n] = \frac{1}{\sqrt{M}} \exp\left\{ j \frac{\pi n^2}{M} \right\}, \tag{1}$$

$$d[n] = u^*[n] = \frac{1}{\sqrt{M}} \exp\left\{ -j \frac{\pi n^2}{M} \right\}, \tag{2}$$

where $n = 0, 1, ..., M-1$ is the sample index.

B. Fundamentals of LoRa and GCSS Modulation

In the conventional LoRa modulation, M orthogonal upchirps are used to represent the message symbols. Every SF information bits $b_0, b_1, ..., b_{SF-1}$ are mapped to a data symbol as

$$m = \sum_{i=0}^{SF-1} b_i 2^i, \tag{3}$$

This article has been accepted for publication in IEEE Internet of Things Journal. This is the author's version which has not been fully edited and content may change prior to final publication. Citation information: DOI 10.1109/JIOT.2024.3486126

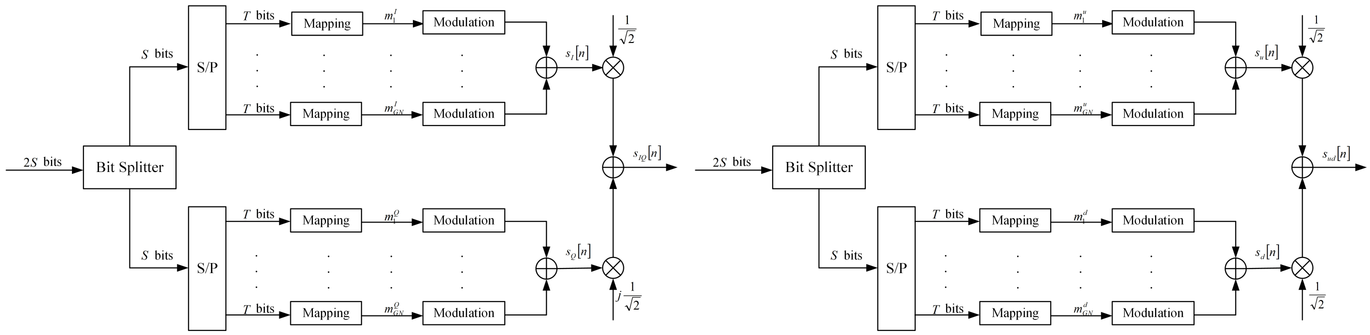

(a) IQ-GCSS (b) TDM-GCSS

Fig. 1. Transmitter architectures of IQ-GCSS modulation and TDM-GCSS modulation.

where $m \in \{0, 1, ..., M-1\}$. Then the transmitted signal is given by

$$s_L[n] = u[n] \exp\left\{ j \frac{2\pi mn}{M} \right\}. \tag{4}$$

Considering $BT_s = M$ where T_s represents the symbol period, the SE of LoRa modulation is given as

$$\eta_L = \frac{R_s \log_2 M}{B} = \frac{SF}{BT_s} = \frac{SF}{2^{SF}}. \tag{5}$$

In GCSS modulation, the available orthogonal upchirps are sequentially divided into GN groups and the number of information bits carried by each independent group becomes

$$T = \log_2 \frac{M}{GN} = SF - \log_2 GN. \tag{6}$$

Therefore, a total of S information bits can be transmitted within each GCSS symbol where $S = GN(SF - \log_2 GN)$. More precisely, the transmitter first divides every S information bits into GN groups, represented by $\boldsymbol{b^k} = [b_0^k, b_1^k, ..., b_{T-1}^k]$, where $k = 1, ..., GN$ is the group index. Then the symbol mapping rule is given as

$$m_k = (k-1)\frac{M}{GN} + \sum_{i=0}^{T-1} b_i^k 2^i, \tag{7}$$

where m_k is the data symbol of the kth group. Finally, multiple orthogonal upchirps in different groups are superimposed together and the transmitted signal is modeled as

$$s_G[n] = \sqrt{\frac{1}{GN}} \sum_{k=1}^{GN} u[n] \exp\left\{ j \frac{2\pi m_k n}{M} \right\}. \tag{8}$$

Therefore, the SE of GCSS modulation is expressed as

$$\eta_G = \frac{S}{M} = \frac{GN(SF - \log_2 GN)}{2^{SF}}. \tag{9}$$

Remark 1: GCSS modulation can be regarded as a more generalized LoRa modulation which can realize a more extensive trade-off between EE and SE to satisfy various IoT applications. Specifically, when $GN = 1$, GCSS modulation will degenerate into the conventional LoRa modulation.

III. System Model

In this section, we present the system model of our proposed IQ-GCSS modulation and TDM-GCSS modulation, including their transmission and detection. Herein, Fig. 1 depicts the transmitter architectures of the two modulation schemes.

A. Transmission

1) IQ-GCSS Modulation: In IQ-GCSS modulation, the information bits are encoded in both in-phase and quadrature components of the transmitted signal. As depicted in Fig. 1(a), the transmitter first splits the transmitted information bits into two sets with each set containing S information bits. After that, the S information bits encoded in the in-phase and quadrature components of the transmitted signal are divided into GN groups. Without loss of generality, we denote $\boldsymbol{b^{I,k}} = [b_0^{I,k}, b_1^{I,k}, ..., b_{T-1}^{I,k}]$ and $\boldsymbol{b^{Q,k}} = [b_0^{Q,k}, b_1^{Q,k}, ..., b_{T-1}^{Q,k}]$ as the GN groups of information bits which are encoded in the in-phase and quadrature components, respectively, where $k = 1, ..., GN$ represents the group index. Then the in-phase and quadrature data symbols m_k^I and m_k^Q can be obtained as

$$m_k^I = (k-1)\frac{M}{GN} + \sum_{i=0}^{T-1} b_i^{I,k} 2^i, \tag{10}$$

$$m_k^Q = (k-1)\frac{M}{GN} + \sum_{i=0}^{T-1} b_i^{Q,k} 2^i. \tag{11}$$

After that, the in-phase and quadrature components of the transmitted signal can be modeled as

$$s_I[n] = \sqrt{\frac{1}{GN}} \sum_{k=1}^{GN} u[n] \exp\left\{ j \frac{2\pi m_k^I n}{M} \right\}, \tag{12}$$

$$s_Q[n] = \sqrt{\frac{1}{GN}} \sum_{k=1}^{GN} u[n] \exp\left\{ j \frac{2\pi m_k^Q n}{M} \right\}. \tag{13}$$

Finally, the transmitted signal of IQ-GCSS modulation is given as

$$s_{IQ}[n] = \frac{1}{\sqrt{2}} (s_I[n] + j s_Q[n]). \tag{14}$$

Therefore, although the in-phase and quadrature components of the transmitted signal are not orthogonal, IQ-GCSS

modulation can transmit twice the number of information bits within each symbol compared to the conventional GCSS modulation.

2) TDM-GCSS Modulation: Similar to IQ-GCSS modulation, a total of $2S$ information bits can be carried by each TDM-GCSS symbol. As illustrated in Fig. 1(b), the transmitted information bits are split into two branches with each branch containing S bits. After that, the S information bits are divided into GN groups, which are encoded in the modulated upchirps and modulated downchirps, respectively. Likewise, we denote $\boldsymbol{b^{u,k}} = [b_0^{u,k}, b_1^{u,k}, ..., b_{T-1}^{u,k}]$ and $\boldsymbol{b^{d,k}} = [b_0^{d,k}, b_1^{d,k}, ..., b_{T-1}^{d,k}]$ as the GN groups of information bits encoded in the upchirps and downchirps, respectively. The corresponding mapping symbols can be obtained as

$$m_k^u = (k-1)\frac{M}{GN} + \sum_{i=0}^{T-1} b_i^{u,k} 2^i, \tag{15}$$

$$m_k^d = (k-1)\frac{M}{GN} + \sum_{i=0}^{T-1} b_i^{d,k} 2^i. \tag{16}$$

Then, the modulated signals in the two branches are given as

$$s_u[n] = \sqrt{\frac{1}{GN}} \sum_{k=1}^{GN} u[n] \exp\left\{ j\frac{2\pi m_k^u n}{M} \right\}, \tag{17}$$

$$s_d[n] = \sqrt{\frac{1}{GN}} \sum_{k=1}^{GN} d[n] \exp\left\{ j\frac{2\pi m_k^d n}{M} \right\}. \tag{18}$$

Finally, the transmitted signal of TDM-GCSS modulation is given by

$$s_{ud}[n] = \frac{1}{\sqrt{2}}(s_u[n] + s_d[n]). \tag{19}$$

Hence, although the modulated upchirps and modulated downchirps are not orthogonal, TDM-GCSS modulation can also transmit twice the number of information bits within each symbol compared to the conventional GCSS modulation.

B. Coherent Detection

The received signal in a frequency-flat fading channel can be expressed as

$$r[n] = hs[n] + w[n] = \alpha e^{j\theta} s[n] + w[n], \tag{20}$$

where h denotes the complex channel gain with $\mathbb{E}\left\{|h|^2\right\} = 1$ and $w[n]$ is the additive white Gaussian noise with zero mean and variance σ^2. Moreover, α and θ represent the channel's magnitude and phase, respectively. For the sake of simplicity, we denote $\boldsymbol{r} = [r[0], ..., r[M-1]]$ and $\boldsymbol{s} = [s[0], ..., s[M-1]]$. The optimal maximum likelihood (ML) estimation of the transmitted data symbols maximizes the likelihood function, which is given by

$$p(\boldsymbol{r}|\boldsymbol{s}, h) = C \exp\left\{ \frac{2\Re\left\{ h^* \sum_{n=0}^{M-1} r[n] s^*[n] \right\}}{\sigma^2} \right\}, \tag{21}$$

where $(\cdot)^*$ and $\Re\{\cdot\}$ denote the complex conjugate and real part extraction operators, respectively, and $C = (\frac{1}{\pi\sigma^2})^M \exp\left\{ -\frac{||\boldsymbol{r}||^2 + \alpha^2 ||\boldsymbol{s}||^2}{\sigma^2} \right\}$.

Note that C is independent of the data symbols, the ML detection can be simplified as

$$\hat{m}_k^{I/u}, \hat{m}_k^{Q/d} = \arg\max \Re\left\{ h^* \sum_{n=0}^{M-1} r[n] s^*[n] \right\}, \tag{22}$$

where $\hat{m}_k^{I/u}$ and $\hat{m}_k^{Q/d}$ represent the estimated data symbols of IQ-GCSS modulation or TDM-GCSS modulation.

1) IQ-GCSS Modulation: Specifically, for IQ-GCSS modulation, we have

$$\begin{aligned} \sum_{n=0}^{M-1} r[n] s^*[n] &= \beta \sum_{k=1}^{GN} \sum_{n=0}^{M-1} r_1[n] \exp\left\{ -j\frac{2\pi m_k^I n}{M} \right\} \\ &\quad - j\beta \sum_{k=1}^{GN} \sum_{n=0}^{M-1} r_1[n] \exp\left\{ -j\frac{2\pi m_k^Q n}{M} \right\} \\ &= \beta R_1[l] - j\beta R_1[l], \end{aligned} \tag{23}$$

where $\beta = \sqrt{\frac{1}{2GN}}$, $r_1[n] = r[n]u^*[n] = r[n]d[n]$, and $R_1[l] = \sum_{k=1}^{GN} R_1[l_k]$ is the M-point DFT of $r_1[n]$ with $l_k \in \left\{ (k-1)\frac{M}{GN}, ..., k\frac{M}{GN} - 1 \right\}$ representing the frequency bin index of the kth group. By substituting (23) into (22), the coherent detection of in-phase and quadrature data symbols reverts to identifying GN peak indexes of the real and imaginary parts of the DFT output, which can be expressed as

$$\hat{m}_k^I = \arg\max_l \Re\left\{ h^* R_1[l] \right\}, l \in \left\{ (k-1)\frac{M}{GN}, ..., k\frac{M}{GN} - 1 \right\} \tag{24}$$

$$\hat{m}_k^Q = \arg\max_l \Im\left\{ h^* R_1[l] \right\}, l \in \left\{ (k-1)\frac{M}{GN}, ..., k\frac{M}{GN} - 1 \right\} \tag{25}$$

where $\Im\{\cdot\}$ denotes the imaginary part extraction operator. In AWGN channel, (24) and (25) can be simplified as

$$\hat{m}_k^I = \arg\max_l \Re\left\{ R_1[l] \right\}, l \in \left\{ (k-1)\frac{M}{GN}, ..., k\frac{M}{GN} - 1 \right\} \tag{26}$$

$$\hat{m}_k^Q = \arg\max_l \Im\left\{ R_1[l] \right\}, l \in \left\{ (k-1)\frac{M}{GN}, ..., k\frac{M}{GN} - 1 \right\} \tag{27}$$

2) TDM-GCSS Modulation: For TDM-GCSS modulation, we have

$$\begin{aligned} \sum_{n=0}^{M-1} r[n] s^*[n] &= \beta \sum_{k=1}^{GN} \sum_{n=0}^{M-1} r_1[n] \exp\left\{ -j\frac{2\pi m_k^u n}{M} \right\} \\ &\quad + \beta \sum_{k=1}^{GN} \sum_{n=0}^{M-1} r_2[n] \exp\left\{ -j\frac{2\pi m_k^d n}{M} \right\} \\ &= \beta R_1[l] + \beta R_2[l], \end{aligned} \tag{28}$$

where $r_2[n] = r[n]d^*[n] = r[n]u[n]$ and $R_2[l] = \sum_{k=1}^{GN} R_2[l_k]$ is the M-point DFT of $r_2[n]$, $l_k \in \left\{ (k-1)\frac{M}{GN}, ..., k\frac{M}{GN} - 1 \right\}$. Consistent with the symbol mapping rules, the corresponding data symbols are estimated as

$$\hat{m}_k^u = \arg\max_l \Re\left\{ h^* R_1[l] \right\}, l \in \left\{ (k-1)\frac{M}{GN}, ..., k\frac{M}{GN} - 1 \right\} \tag{29}$$

$$\hat{m}_k^d = \arg\max_l \Re\left\{h^* R_2[l]\right\}, l \in \left\{(k-1)\frac{M}{GN}, ..., k\frac{M}{GN} - 1\right\} \tag{30}$$

Likewise, in AWGN channel, (29) and (30) can be simplified as

$$\hat{m}_k^u = \arg\max_l \Re\left\{R_1[l]\right\}, l \in \left\{(k-1)\frac{M}{GN}, ..., k\frac{M}{GN} - 1\right\} \tag{31}$$

$$\hat{m}_k^d = \arg\max_l \Re\left\{R_2[l]\right\}, l \in \left\{(k-1)\frac{M}{GN}, ..., k\frac{M}{GN} - 1\right\} \tag{32}$$

Remark 2: In practice, accurate channel state information is required for coherent detection at the receiver. As a result, channel estimation and equalization are necessary before demodulation, which could considerably increase the receiver's complexity and thus not be feasible for many low-cost IoT devices. Therefore, non-coherent detection is more attractive in the context of IoT applications and we mainly consider non-coherent detection in the sequel.

C. Non-coherent Detection

By deeply investigating the symbol decision metrics, we develop non-coherent detection methods for both IQ-GCSS modulation and TDM-GCSS modulation.

1) IQ-GCSS Modulation: For IQ-GCSS modulation, $R_1[l]$ is calculated as

$$\begin{aligned} R_1[l] &= \sum_{n=0}^{M-1} r[n]d[n] \exp\left\{-j\frac{2\pi ln}{M}\right\} \\ &= \alpha e^{j\theta} \sum_{n=0}^{M-1} s[n]d[n] \exp\left\{-j\frac{2\pi ln}{M}\right\} + \bar{W}[l], \end{aligned} \tag{33}$$

where $\bar{W}[l] = \sum_{n=0}^{M-1} w[n]d[n] \exp\left\{-j\frac{2\pi ln}{M}\right\} \sim \mathcal{CN}(0, \sigma^2)$. Moreover, we have

$$s[n]d[n] = \frac{\beta}{M} \sum_{k=1}^{GN} \exp\left\{j\frac{2\pi m_k^I n}{M}\right\} + j \exp\left\{j\frac{2\pi m_k^Q n}{M}\right\}. \tag{34}$$

By substituting (34) into (33), $R_1[l]$ can be expressed as

$$R_1[l] = \alpha\beta e^{j\theta} \sum_{k=1}^{GN} \left(\delta[l_k - m_k^I] + j\delta[l_k - m_k^Q]\right) + \bar{W}[l], \tag{35}$$

where $\delta[\cdot]$ represents the Kronecker delta function. It can be observed that the channel phase will rotate the IQ components and lead to symbol decision error when h is unknown at the receiver. Nevertheless, non-coherent detection can be performed for each independent group. Take the first group as an example, we have

$$R_1[l_1] = \alpha\beta e^{j\theta} \left(\delta[l_1 - m_1^I] + j\delta[l_1 - m_1^Q]\right) + \bar{W}[l_1], \tag{36}$$

where $l_1 \in \left\{0, ..., \frac{M}{GN} - 1\right\}$. Therefore, when $m_1^I = m_1^Q$, we have

$$|R_1[l_1]| = \begin{cases} \left|\sqrt{2}\alpha\beta e^{j\theta} e^{j\frac{\pi}{4}} + \bar{W}[m_1^I]\right|, & \text{if } l_1 = m_1^I = m_1^Q \\ \left|\bar{W}[l_1]\right|, & \text{otherwise.} \end{cases} \tag{37}$$

Algorithm 1 Non-coherent Detection for IQ-GCSS Modulation

Input: $r[n], u[n]$ for $n = 0, 1, ..., M-1$, GN, Ξ
Output: $\hat{m}_k^I, \hat{m}_k^Q$ for $k = 1, ..., GN$

```
Compute R_1[l] = DFT(r[n]u*[n]) for n = 0, 1, ..., M-1
for k = 1, ..., GN do
    S ← {(k-1) M/GN, ..., k M/GN - 1}
    l_k^a, l_k^b = arg max_{l∈S} |R_1[l]|, l_k^a ≠ l_k^b
    Compute Λ = |R_1[l_k^a]| / |R_1[l_k^b]|
    if Λ ≥ Ξ then
        m̂_k^I = m̂_k^Q = l_k^a
    else
        Compute ψ = ∠{R_1[l_k^a]* R_1[l_k^b]}
        if 0 ≤ ψ < π then
            m̂_k^I = l_k^a , m̂_k^Q = l_k^b
        else
            m̂_k^I = l_k^b , m̂_k^Q = l_k^a
        end if
    end if
end for
return m̂_k^I, m̂_k^Q for k = 1, ..., GN
```

Otherwise, when $m_1^I \neq m_1^Q$, $|R_1[l_1]|$ is given as

$$|R_1[l_1]| = \begin{cases} \left|\alpha\beta e^{j\theta} + \bar{W}[m_1^I]\right|, & \text{if } l_1 = m_1^I \\ \left|\alpha\beta e^{j\theta} e^{j\frac{\pi}{2}} + \bar{W}[m_1^Q]\right|, & \text{if } l_1 = m_1^Q \\ \left|\bar{W}[l_1]\right|, & \text{otherwise.} \end{cases} \tag{38}$$

Following a similar approach in [28], we first extract the indexes of the two largest peaks of $|R_1[l_1]|$, which can be expressed as

$$l_1^a, l_1^b = \arg\max |R_1[l_1]|, \tag{39}$$

where $|R_1[l_1^a]| \geq \left|R_1[l_1^b]\right|$, $l_1^a \neq l_1^b$. It can be observed from (37) and (38) that when $m_1^I = m_1^Q$, we have $|R_1[l_1^a]| \gg \left|R_1[l_1^b]\right|$; otherwise, we have $|R_1[l_1^a]| \approx \left|R_1[l_1^b]\right|$.

To distinguish between the two cases, we define the ratio of $|R_1[l_1^a]|$ and $\left|R_1[l_1^b]\right|$ as the decision metric to compare with a predefined threshold Ξ ($\Xi > 1$). If $\frac{|R_1[l_1^a]|}{|R_1[l_1^b]|} \geq \Xi$, then $m_1^I = m_1^Q$, we have the estimated data symbols $\hat{m}_1^I = \hat{m}_1^Q = l_1^a$ in this case. By contrast, if $1 \leq \frac{|R_1[l_1^a]|}{|R_1[l_1^b]|} < \Xi$, then $m_1^I \neq m_1^Q$, we need to associate the in-phase and quadrature data symbol to the corresponding peak index. To this end, we compute the angle

$$\psi = \angle\left\{R_1[l_1^a]^* R_1[l_1^b]\right\}, \tag{40}$$

where $\angle\{\cdot\}$ represents the angle of a complex variable and $\psi \in [-\pi, \pi)$. According to (36), when $l_1^a = m_1^I$ and $l_1^b = m_1^Q$, we have $\psi = \pi/2$ in the absence of noise; when $l_1^a = m_1^Q$ and $l_1^b = m_1^I$, we have $\psi = -\pi/2$ in the absence of noise. Therefore, the symbol decision in this case can be formulated as $\hat{m}_1^I = l_1^a$ and $\hat{m}_1^Q = l_1^b$ if $0 \leq \psi < \pi$ while $\hat{m}_1^I = l_1^b$ and $\hat{m}_1^Q = l_1^a$ if $-\pi \leq \psi < 0$.

Following the same process, the data symbols for the other groups can be determined subsequently. The complete non-coherent detection algorithm for IQ-GCSS modulation is

presented in Algorithm 1.

2) TDM-GCSS Modulation: For TDM-GCSS modulation, $R_1[l]$ is calculated as

$$\begin{aligned} R_1[l] &= \sum_{n=0}^{M-1} r[n]d[n]\exp\left\{-j\frac{2\pi ln}{M}\right\} \\ &= \alpha\beta e^{j\theta}\sum_{k=1}^{GN}\delta[l_k - m_k^u] + \frac{\alpha\beta e^{j\theta}}{M}\sum_{k=1}^{GN} I_k^d + \bar{W}[l], \end{aligned} \tag{41}$$

where $\bar{W}[l] = \sum_{n=0}^{M-1} w[n]d[n]\exp\left\{-j\frac{2\pi ln}{M}\right\} \sim \mathcal{CN}(0,\sigma^2)$ and $I_k^d = \sum_{n=0}^{M-1}\exp\left\{j\frac{\pi}{M}[2n(m_k^d - l_k) - 2n^2]\right\}$ represents the interference regarding the symbol detection of the modulated upchirps.

Notably, the closed-form expression of I_k^d can be expressed as

$$I_k^d = \begin{cases} 0, & \text{if } |m_k^d - l_k| \text{ is odd} \\ 2\sqrt{\frac{M}{2}}\mathcal{B}, & \text{if } |m_k^d - l_k| \text{ is even} \end{cases} \tag{42}$$

where $\mathcal{B} = \exp\left\{-j\frac{\pi}{4}\right\}\exp\left\{j\frac{\pi}{2M}(m_k^d - l_k)^2\right\}$. The detailed derivation of (42) is presented in Appendix.

Likewise, $R_2[l]$ is calculated as

$$\begin{aligned} R_2[l] &= \sum_{n=0}^{M-1} r[n]u[n]\exp\left\{-j\frac{2\pi ln}{M}\right\} \\ &= \alpha\beta e^{j\theta}\sum_{k=1}^{GN}\delta[l_k - m_k^d] + \frac{\alpha\beta e^{j\theta}}{M}\sum_{k=1}^{GN} I_k^u + \dot{W}[l], \end{aligned} \tag{43}$$

where $\dot{W}[l] = \sum_{n=0}^{M-1} w[n]u[n]\exp\left\{-j\frac{2\pi ln}{M}\right\} \sim \mathcal{CN}(0,\sigma^2)$ and $I_k^u = \sum_{n=0}^{M-1}\exp\left\{j\frac{\pi}{M}[2n^2 + 2n(m_k^u - l_k)]\right\}$ represents the interference with respect to the symbol detection of the modulated downchirps.

Moreover, the closed-form expression of I_k^u is given as

$$I_k^u = \begin{cases} 0, & \text{if } |m_k^d - l_k| \text{ is odd} \\ 2\sqrt{\frac{M}{2}}\mathcal{D}, & \text{if } |m_k^d - l_k| \text{ is even} \end{cases} \tag{44}$$

where $\mathcal{D} = \exp\left\{j\frac{\pi}{4}\right\}\exp\left\{-j\frac{\pi}{2M}(m_k^u - l_k)^2\right\}$. The detailed derivation of (44) can also be seen in Appendix.

Similarly, the non-coherent symbol detection can be performed separately for each independent group in TDM-GCSS modulation. The mapping symbols can be determined as

$$\hat{m}_k^u = \arg\max_l |R_1[l]|, l \in \left\{(k-1)\frac{M}{GN}, ..., k\frac{M}{GN} - 1\right\} \tag{45}$$

$$\hat{m}_k^d = \arg\max_l |R_2[l]|, l \in \left\{(k-1)\frac{M}{GN}, ..., k\frac{M}{GN} - 1\right\} \tag{46}$$

Compared to the conventional GCSS modulation, the interference term appears during the symbol detection in TDM-GCSS modulation due to the loss of orthogonality between the modulated upchirps and modulated downchirps, which may have a negative impact on the BER performance. Take the first group as an example, we have

$$R_1[l_1] = \underbrace{\alpha\beta e^{j\theta}\delta[l_1 - m_1^u]}_{\text{signal term}} + \underbrace{\frac{\alpha\beta e^{j\theta}}{M} I_1^d}_{\text{interference term}} + \underbrace{\bar{W}[l_1]}_{\text{noise term}}, \tag{47}$$

$$R_2[l_1] = \underbrace{\alpha\beta e^{j\theta}\delta[l_1 - m_1^d]}_{\text{signal term}} + \underbrace{\frac{\alpha\beta e^{j\theta}}{M} I_1^u}_{\text{interference term}} + \underbrace{\dot{W}[l_1]}_{\text{noise term}}. \tag{48}$$

Nevertheless, according to (42) and (44), the interference term is proportional to $\sqrt{\frac{2}{M}}$, which means each independent group is asymptotically orthogonal as M tends to infinity (e.g., $\sqrt{\frac{2}{M}} \leq 0.25$ for $M \geq 32$) and thus the effect of interference can be negligible.

IV. Performance Analysis

A. BER Analysis

The closed-form approximations for symbol error rate (SER) of LoRa modulation considering non-coherent detection over AWGN and Rayleigh fading channels are given by [5]

$$P_{s,L}^A \approx Q\left(\frac{\sqrt{\gamma_s} - ((H_{M-1})^2 - \frac{\pi^2}{12})^{\frac{1}{4}}}{\sqrt{H_{M-1} - ((H_{M-1})^2 - \frac{\pi^2}{12})^{\frac{1}{2}} + 0.5}}\right), \tag{49}$$

and

$$\begin{aligned} P_{s,L}^R \approx\ & Q\left(-\sqrt{2H_{M-1}}\right) - \sqrt{\frac{\gamma_s}{\gamma_s+1}}\exp\left(-\frac{H_{M-1}}{\gamma_s+1}\right) \\ & \times Q\left(-\sqrt{\frac{2H_{M-1}\gamma_s}{\gamma_s+1}}\right), \end{aligned} \tag{50}$$

respectively, where $\gamma_s = 1/\sigma^2$ represents the effective SNR, $Q(x) = \frac{1}{\sqrt{2\pi}}\int_x^\infty \exp\left(-\frac{u^2}{2}\right)du$ and $H_N = \sum_{i=1}^N \frac{1}{i}$ is the Nth harmonic number.

Based on (49) and (50), the closed-form BER expressions of LoRa modulation in both cases are given as

$$P_{b,L}^A = \kappa_L P_{s,L}^A, \tag{51}$$

$$P_{b,L}^R = \kappa_L P_{s,L}^R, \tag{52}$$

where $\kappa_L = \frac{M}{2(M-1)}$. It can be observed that the BER performance of LoRa modulation can be viewed as functions of M and γ_s. To obtain the closed-form expressions for BER performance of our proposed modulation schemes, we only need to investigate the bit error probability of one group since the symbol detection is performed separately for each independent group.

Specifically, for GCSS modulation, the closed-form approximations for its BER performance considering non-coherent detection over AWGN and Rayleigh fading channels are given by

$$P_{b,G}^A \approx \kappa_G Q\left(\frac{\sqrt{\frac{\gamma_s}{GN}} - ((H_{\frac{M}{GN}-1})^2 - \frac{\pi^2}{12})^{\frac{1}{4}}}{\sqrt{H_{\frac{M}{GN}-1} - ((H_{\frac{M}{GN}-1})^2 - \frac{\pi^2}{12})^{\frac{1}{2}} + 0.5}}\right), \tag{53}$$

and

$$\begin{aligned} P_{b,G}^R \approx \kappa_G\Bigg[& Q\left(-\sqrt{2H_{\frac{M}{GN}-1}}\right) - \sqrt{\frac{\gamma_s}{\gamma_s + GN}} \\ & \times \exp\left(-\frac{H_{\frac{M}{GN}-1}}{\frac{\gamma_s}{GN}+1}\right) Q\left(-\sqrt{\frac{2H_{\frac{M}{GN}-1}\gamma_s}{\gamma_s + GN}}\right)\Bigg], \end{aligned} \tag{54}$$

TABLE II
TIME COMPLEXITY OF SYMBOL DETECTION

Modulation Schemes	Coherent Detection	Non-coherent Detection
LoRa	$\mathcal{O}\left(M + M\log_2 M\right)$	$\mathcal{O}\left(M + M\log_2 M\right)$
GCSS	$\mathcal{O}\left(M + M\log_2 M\right)$	$\mathcal{O}\left(M + M\log_2 M\right)$
IQ-GCSS	$\mathcal{O}\left(M + M\log_2 M\right)$	$\mathcal{O}\left(M + M\log_2 M\right)$
TDM-GCSS	$\mathcal{O}\left(2M + 2M\log_2 M\right)$	$\mathcal{O}\left(2M + 2M\log_2 M\right)$

respectively, where $\kappa_G = \frac{M}{2(M-GN)}$.

Likewise, for IQ-GCSS modulation and TDM-GCSS modulation, the closed-form approximations for their BER performance considering non-coherent detection over AWGN and Rayleigh fading channels are given by

$$P_b^A \approx \kappa_G Q\left(\frac{\sqrt{\frac{\gamma_s}{2GN}} - ((H_{\frac{M}{GN}-1})^2 - \frac{\pi^2}{12})^{\frac{1}{4}}}{\sqrt{H_{\frac{M}{GN}-1} - ((H_{\frac{M}{GN}-1})^2 - \frac{\pi^2}{12})^{\frac{1}{2}} + 0.5}}\right), \tag{55}$$

and

$$P_b^R \approx \kappa_G \Bigg[Q\left(-\sqrt{2H_{\frac{M}{GN}-1}}\right) - \sqrt{\frac{\gamma_s}{\gamma_s + 2GN}} \times \exp\left(-\frac{H_{\frac{M}{GN}-1}}{\frac{\gamma_s}{2GN}+1}\right) Q\left(-\sqrt{\frac{2H_{\frac{M}{GN}-1}\gamma_s}{\gamma_s + 2GN}}\right)\Bigg], \tag{56}$$

respectively. It can be observed that the BER performance of GCSS, IQ-GCSS, and TDM-GCSS can be regarded as functions of M, γ_s, and GN.

Remark 3: Although the two branches of IQ-GCSS modulation (i.e., in-phase and quadrature components) and TDM-GCSS modulation (i.e., modulated upchirps and modulated downchirps) are not orthogonal, the interference can be negligible as M tends to infinity, which means their BER performance can be lower bounded by that of $\frac{M}{GN}$-ary orthogonal modulation. Consequently, the BER performance of IQ-GCSS modulation and TDM-GCSS modulation can be approximated by that of GCSS modulation with effective SNR being $\frac{\gamma_s}{2GN}$.

B. Complexity Analysis

To analyze the computational complexity of demodulation, the symbol detection can be divided into three phases, namely, dechirp, DFT, and frequency domain (FD) peak index decision [13], [21]. Since the main computational complexity arises from the dechirp and DFT operations, a detailed time complexity analysis of our proposed modulation schemes is demonstrated in Table II, expressed in the order of required complex multiplications. It can be observed that LoRa, GCSS, and IQ-GCSS have a similar time complexity for both coherent and non-coherent detection which can be simplified as $\mathcal{O}\left(M\log_2 M\right)$ since only one dechirp and DFT operation is performed during the demodulation. TDM-GCSS modulation has a higher complexity since two dechirp and DFT operations are needed during the symbol detection. However, the increase of complexity is not significant compared to the improvement of SE and data rate. Moreover, it should be noted that for coherent detection, channel estimation and equalization are needed before demodulation, which could considerably increase the computational complexity for many resource-constrained IoT devices.

V. NUMERICAL RESULTS AND DISCUSSION

In this section, we provide an overall performance evaluation of our proposed modulation schemes through numerical simulations. The conventional LoRa modulation, IQ-CSS modulation, TDM-LoRa modulation, and GCSS modulation are considered as benchmarks for comparison. Without loss of generality, we define the EE as the required E_b/N_0 for correct detection at a given BER level. Unless otherwise specified, we set $B = 125$ kHz, $SF = 11$, and $GN = 2$ in our simulations.[3]

A. SE versus EE Performance Comparison

For a fair comparison of our proposed modulation schemes and the traditional LoRa modulation with the same SE, we adopt the same method as in [28] to evaluate the SE versus EE performance. Specifically, for a given SE, the EE is obtained by evaluating the required E_b/N_0 to reach a BER level of 10^{-3}. Fig. 2 presents the SE versus EE performance of our proposed modulation schemes and the traditional LoRa modulation, where the numercal results are obtained considering non-coherent detection over AWGN channels. It can be observed that both the SE and the required E_b/N_0 decrease with the increase of SF. Moreover, our proposed modulation schemes outperform the traditional LoRa modulation since both IQ-GCSS modulation and TDM-GCSS modulation require lower E_b/N_0 for the same SE, which means a higher EE relative to the conventional LoRa modulation. In addition, it can be observed that for smaller SFs, i.e., $SF = 7, 8, 9$, IQ-GCSS modulation performs better than TDM-GCSS modulation whereas for larger SFs, i.e., $SF = 10, 11, 12$, TDM-GCSS modulation performs better than IQ-GCSS modulation.

[3]In practice, both SF and GN can be configured according to the specific requirements of IoT applications in terms of coverage and data rate. Specifically, smaller SF and larger GN will lead to a higher data rate and reduced coverage, and vice versa.

This article has been accepted for publication in IEEE Internet of Things Journal. This is the author's version which has not been fully edited and content may change prior to final publication. Citation information: DOI 10.1109/JIOT.2024.3486126

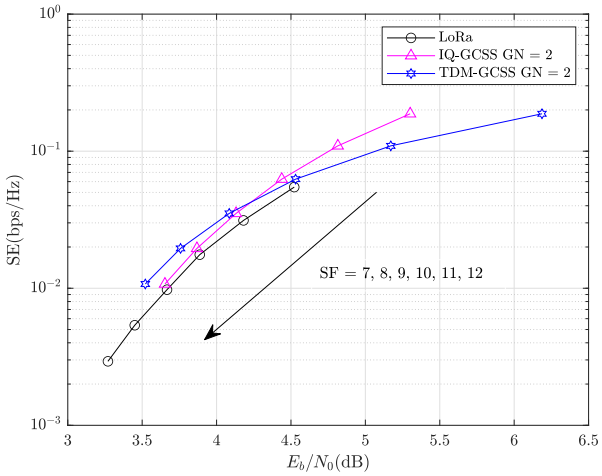

Fig. 2. SE versus EE performance for LoRa, IQ-GCSS, and TDM-GCSS considering non-coherent detection.

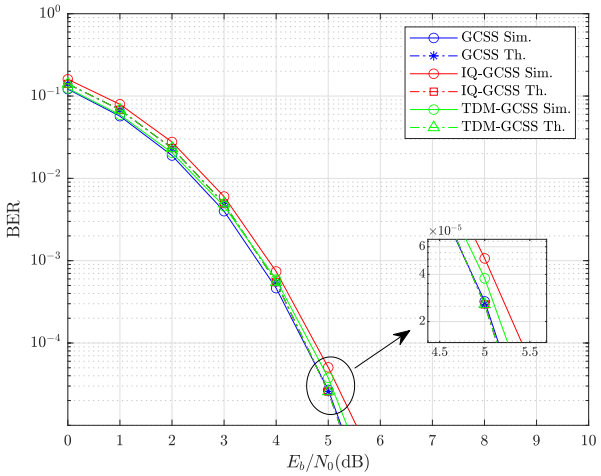

(a) AWGN channel

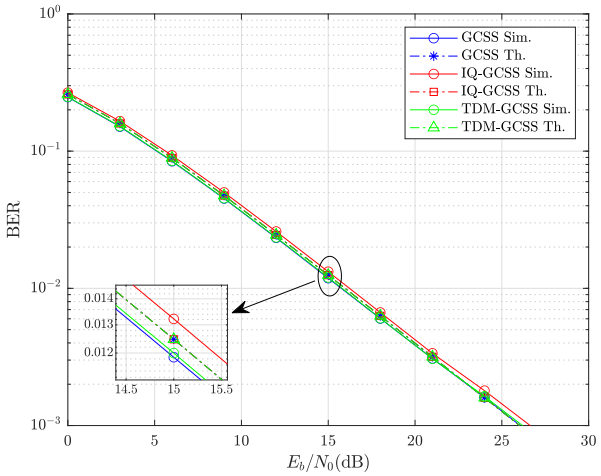

(b) Rayleigh fading channel

Fig. 3. BER performance of GCSS, IQ-GCSS, and TDM-GCSS over both AWGN and Rayleigh fading channels considering non-coherent detection.

B. BER Performance Comparison

Fig. 3 shows the BER performance of GCSS modulation, IQ-GCSS modulation, and TDM-GCSS modulation considering non-coherent detection over both AWGN and Rayleigh fading channels. The notations 'Th.' and 'Sim.' denote the theoretical and numerical results, respectively. In the case of AWGN channels, the theoretical curves in Fig. 3(a) are obtained using (53) and (55) while in the case of Rayleigh fading channels, the theoretical curves in Fig. 3(b) are obtained using (54) and (56), respectively. It can be seen that the theoretical BER curves agree well with the simulated ones in both cases, which substantially verifies the accuracy of our analysis.

C. BER and Throughput Over AWGN Channels

Fig. 4(a) presents the BER of different modulation schemes over AWGN channels considering non-coherent detection. It can be seen that the conventional LoRa modulation achieves the best BER performance. A marginal performance degradation can be observed for our proposed modulation schemes when compared to the conventional LoRa modulation. In particular, the performance loss is around 0.25 dB for GCSS modulation, 0.35 dB for TDM-GCSS modulation, and 0.55 dB for IQ-GCSS modulation ($\Xi = 2.2$)[4] at the BER level of 10^{-5}.

Moreover, to illustrate the advantages of our proposed schemes more intuitively, Fig. 4(b) depicts the effective throughput versus E_b/N_0 for these modulation schemes. Specifically, the theoretical bit rate of a LoRa-like modulation scheme is given by ηB with η denoting the SE of the considered modulation scheme. To be noticed, the actual bit rate is also related to the BER for a given SNR. Therefore, the effective throughput ρ (bps) is given by

$$\rho = \eta B(1 - BER), \tag{57}$$

[4]It should be noted that different values of Ξ could lead to different BER performance of IQ-GCSS modulation.

which is adopted in LoRa systems for practical performance evaluation [12], [18].

As shown in Fig. 4(b), our proposed modulation schemes achieve a noteworthy performance gain in terms of effective throughput compared to the classical counterparts. Specifically, the effective throughput of IQ-GCSS modulation and TDM-GCSS modulation doubles that of the original GCSS modulation. Moreover, the effective throughput of IQ-GCSS modulation and TDM-GCSS modulation is also nearly four times that of the conventional LoRa modulation when $GN = 2$. Therefore, the BER degradation of our proposed schemes can be well justified by their performance improvements in the SE and data rate. Its significance can be elaborated as follows.

From the network perspective, as the link-level data rate increases, the time-on-air (ToA) of a fixed-length packet decreases, which improves transmission efficiency and reduces the probability of packet collisions, which significantly enhances the scalability of LoRa network [30]. From the

This article has been accepted for publication in IEEE Internet of Things Journal. This is the author's version which has not been fully edited and content may change prior to final publication. Citation information: DOI 10.1109/JIOT.2024.3486126

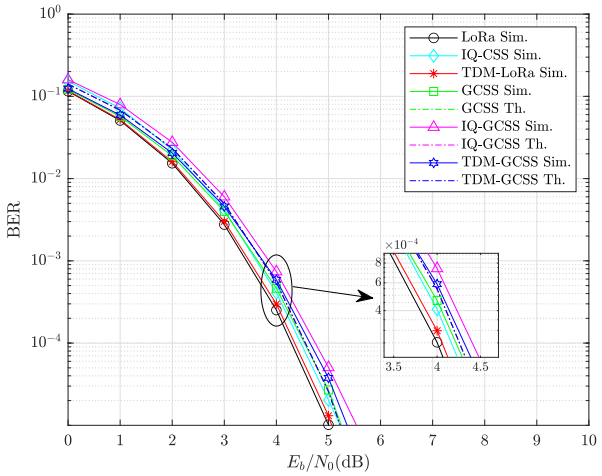

(a) BER

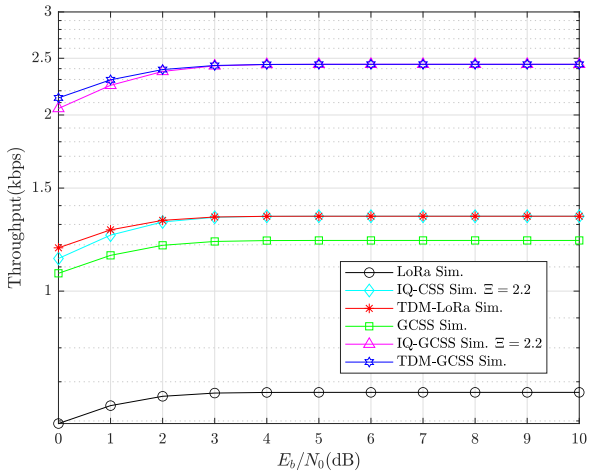

(b) Effective Throughput

Fig. 4. BER and Effective throughput of different modulation schemes over AWGN channels considering non-coherent detection.

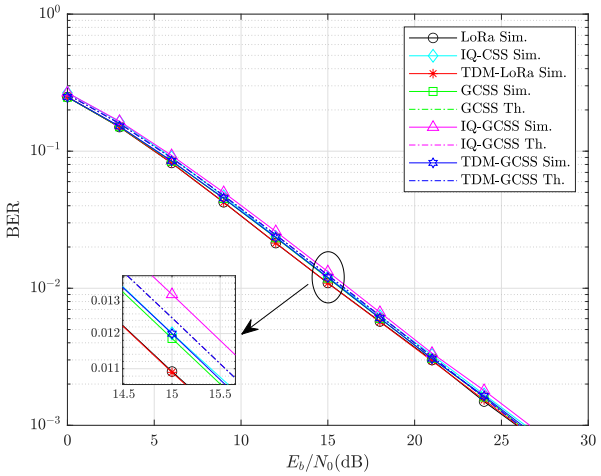

(a) BER

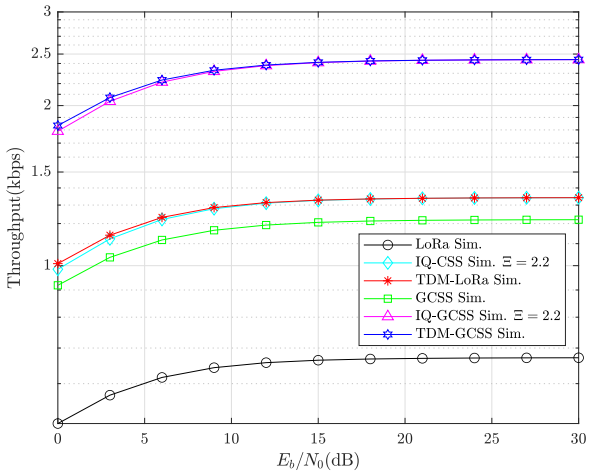

(b) Effective Throughput

Fig. 5. BER and Effective throughput of different modulation schemes over Rayleigh fading channels considering non-coherent detection.

application perspective, the decreased ToA reduces the energy consumption for end devices and thus extends their battery life, which contributes to the long life expectancy of IoT network. In our opinion, the key challenge of implementing IQ-GCSS and TDM-GCSS in the existing LPWAN infrastructure is that they are not fully compatible with the conventional LoRa modulation. Specifically, the transceiver architectures need to be redesigned for practical implementation, which may limit their wide deployment. Nevertheless, they can be customized to satisfy some specific application scenarios which extends the application scope of LoRa technology. Moreover, it can be expected that network upgrade is necessary to accommodate the ever-increasing transmission demands of heterogeneous IoT applications such as image transmission [31] and industrial IoT [32] where our proposed modulation schemes can serve as potential candidates.

D. BER and Throughput Over Rayleigh Fading Channels

Fig. 5 demonstrates the BER and effective throughput of different modulation schemes over Rayleigh fading channels considering non-coherent detection. It can be observed from Fig. 5(a) that the BER curves for different modulation schemes appear very close to each other. The BER performance loss of our proposed schemes is within 1 dB. Moreover, as illustrated in Fig. 5(b), our proposed IQ-GCSS modulation and TDM-GCSS modulation still achieve a noteworthy throughput gain compared to the classical counterparts. Nonetheless, by inspecting Fig. 4(a) and Fig. 5(a), one can see that the Rayleigh fading environment results in a considerable BER performance loss, which boils down to the degradation of EE and coverage. Therefore, it's very essential to cope with the severe performance loss in Rayleigh fading channels, where the reliability of communications can be enhanced using suitable channel coding schemes [33], [34]. For example,

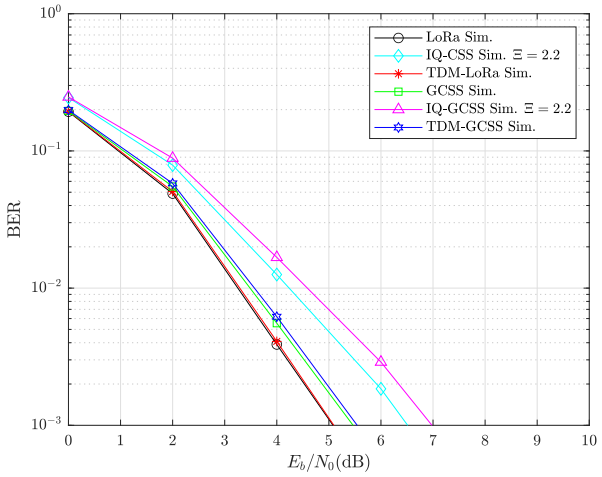

(a) BER

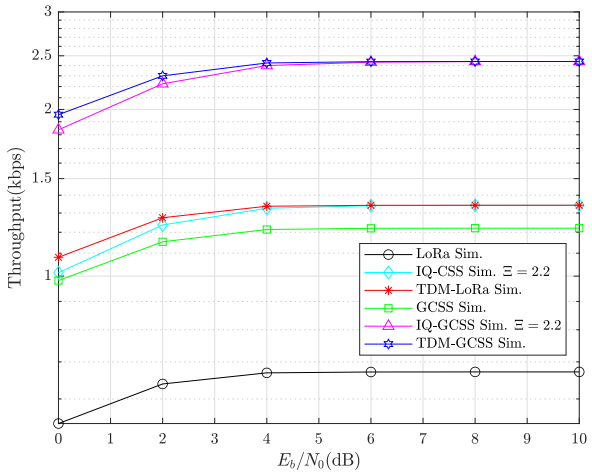

(b) Effective Throughput

Fig. 6. BER and Effective throughput of different modulation schemes over frequency-selective fading channels considering non-coherent detection.

Turbo code [35] and low-density parity-check (LDPC) code [36] have been proposed to improve the BER performance of LoRa-like modulation schemes.

E. BER and Throughput Over Frequency-Selective Fading Channels

In this section, we consider the BER and effective throughput of our proposed modulation schemes over a simple frequency-selective fading channel with impulse response of $h[n] = \sqrt{0.8}\delta[n] + \sqrt{0.2}\delta[n-1]$ [3], [37]. As shown in Fig. 6(a), the BER performance loss of both GCSS modulation and TDM-GCSS modulation is still acceptable. However, IQ-CSS modulation and IQ-GCSS modulation are shown to be more sensitive to frequency-selective fading caused by multi-path propagation. For a target BER of 10^{-3}, the BER degradation of IQ-CSS modulation and IQ-GCSS modulation relative to the conventional LoRa modulation is around 1.5 dB and 2 dB, respectively. Nevertheless, as shown in Fig. 6(b), significant effective throughput improvements of our proposed modulation schemes can still be achieved compared to the classical counterparts.

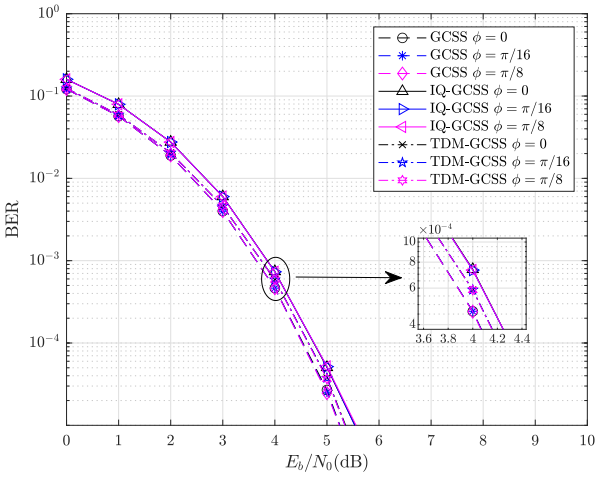

Fig. 7. BER performance of GCSS, IQ-GCSS, and TDM-GCSS with phase offsets considering non-coherent detection.

F. BER Performance Considering Phase Offset

In this section, the BER performance of our proposed modulation schemes considering the impact of phase offset is investigated. The received signal corrupted by phase offset over an AWGN channel can be given as $r[n] = s[n]\exp\{j\phi\} + w[n]$, where ϕ denotes the phase offset. Herein, Fig. 7 depicts the BER performance of GCSS modulation, IQ-GCSS modulation, and TDM-GCSS modulation with phase offsets. Note that we still set $\Xi = 2.2$ to obtain the simulation results of IQ-GCSS modulation. It can be easily observed that the BER performance in the presence of phase offset is identical to that of $\phi = 0$, which demonstrates the robustness of our proposed modulation schemes to phase offset.

G. BER Performance Considering Multi-user Interference

Due to the fact that ALOHA-based MAC protocol is adopted for LoRa network, the transmitted data packets are inevitably exposed to collisions with the high density of IoT devices. Since different SFs are quasi-orthogonal, how to deal with the interference in case of packet collisions with the same SF is the biggest challenge [38]. Herein, Fig. 8 presents the performance comparison of LoRa modulation, GCSS modulation, IQ-GCSS modulation, and TDM-GCSS modulation considering multi-user interference. For a fair comparison, the signal-to-interference ratio (SIR) is set to be 6 dB, which is typically considered to be the SIR demodulation threshold due to the capture effect [39], [40]. As shown in Fig. 8, the performance loss is around 2.3 dB for LoRa modulation, 2.5 dB for GCSS modulation, 3.2 dB for IQ-GCSS modulation, and 2.7 dB for TDM-GCSS modulation at the BER level of 10^{-4}. Although the performance loss of our proposed modulation schemes is slightly worse than the

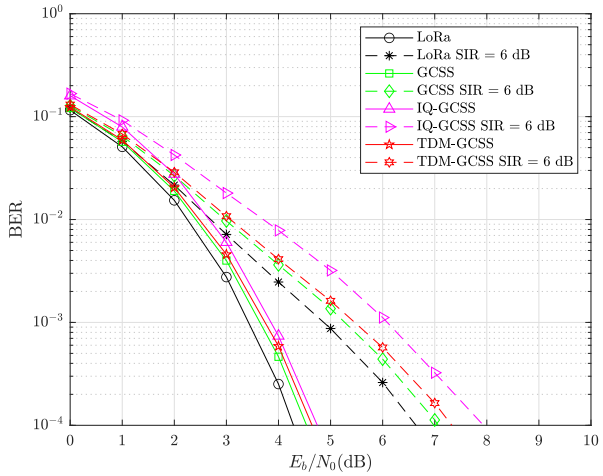

Fig. 8. Performance comparison of LoRa, GCSS, IQ-GCSS, and TDM-GCSS considering the impact of multi-user interference.

conventional LoRa modulation, the BER degradation is still acceptable. In particular, the effective throughput gains of our proposed modulation schemes still make them more advantageous than the conventional LoRa modulation. However, it should be noted that the link-level performance of CSS-based communication systems deteriorates rapidly with the decrease of SIR, which could result in a limited network capacity [41]. To deal with this problem, the promising solutions can be considered from two aspects, namely link coordination [42] and multi-user detection [43], [44], which still need further research in the future.

VI. Conclusion

In this paper, we have proposed two enhanced group-based CSS modulation schemes, namely IQ-GCSS modulation and TDM-GCSS modulation, which can further enhance the SE and data rate compared to the classical counterparts. The transmitter architectures of our proposed schemes have been presented along with both coherent and non-coherent detection methods. Moreover, an overall performance analysis of our proposed schemes has been provided in terms of BER and demodulation complexity. Numerical results not only validate the accuracy of our theoretical analysis but also demonstrate that our proposed schemes significantly outperform the classical counterparts in terms of effective throughput. For future research, it's very interesting to investigate the multi-user detection from the PHY layer perspective and the link coordination from the MAC layer perspective to further enhance the performance in an interference-dominated scenario.

Appendix

Derivation of Eq. (42) and Eq. (44)

The generalized quadratic Gauss sum is given by

$$G(a,b,c)=\sum_{n=0}^{|c|-1}\exp\left\{j\frac{\pi}{c}(an^2+bn)\right\}, \tag{58}$$

where a,b,c are integers with $ac\neq 0$ and $ac+b$ is even. According to the reciprocity theorem for Gauss sums [45], we have

$$\begin{aligned}G(a,b,c)=&\sqrt{|\frac{c}{a}|}\exp\left\{j\frac{\pi}{4ac}(|ac|-b^2)\right\}\\&\sum_{n=0}^{|a|-1}\exp\left\{-j\frac{\pi}{a}(bn+cn^2)\right\}.\end{aligned} \tag{59}$$

Therefore, for $I_k^d=\sum_{n=0}^{M-1}\exp\left\{j\frac{\pi}{M}[2n(m_k^d-l_k)-2n^2]\right\}$ we have $a=-2$, $b=2(m_k^d-l_k)$, $c=M$ and it can be computed as

$$\begin{aligned}I_k^d&=\sum_{n=0}^{M-1}\exp\left\{j\frac{\pi}{M}[2n(m_k^d-l_k)-2n^2]\right\}\\&=\sqrt{\frac{M}{2}}\exp\left\{j\frac{\pi}{-8M}[2M-4(m_k^d-l_k)^2]\right\}\mathcal{A},\end{aligned} \tag{60}$$

where

$$\begin{aligned}\mathcal{A}&=\sum_{n=0}^{1}\exp\left\{j\frac{\pi}{2}[Mn^2+2(m_k^d-l_k)n]\right\}\\&=1+\exp\left\{j\pi(m_k^d-l_k)\right\}.\end{aligned} \tag{61}$$

As a result, if $|m_k^d-l_k|$ is odd, then $\mathcal{A}=0$, which leads to $I_k^d=0$; if $|m_k^d-l_k|$ is even, then $\mathcal{A}=2$ and I_k^d can be further simplified as

$$\begin{aligned}I_k^d&=2\sqrt{\frac{M}{2}}\exp\left\{-j\frac{\pi}{4}\right\}\exp\left\{j\frac{\pi}{2M}(m_k^d-l_k)^2\right\}\\&=2\sqrt{\frac{M}{2}}\mathcal{B},\end{aligned} \tag{62}$$

where $\mathcal{B}=\exp\left\{-j\frac{\pi}{4}\right\}\exp\left\{j\frac{\pi}{2M}(m_k^d-l_k)^2\right\}$.

Similarly, we have $a=2$, $b=2(m_k^u-l_k)$, $c=M$ for $I_k^u=\sum_{n=0}^{M-1}\exp\left\{j\frac{\pi}{M}[2n^2+2n(m_k^u-l_k)]\right\}$ and it can be computed as

$$\begin{aligned}I_k^u&=\sum_{n=0}^{M-1}\exp\left\{j\frac{\pi}{M}[2n^2+2n(m_k^u-l_k)]\right\}\\&=\sqrt{\frac{M}{2}}\exp\left\{j\frac{\pi}{8M}[2M-4(m_k^u-l_k)^2]\right\}\mathcal{C},\end{aligned} \tag{63}$$

where

$$\begin{aligned}\mathcal{C}&=\sum_{n=0}^{1}\exp\left\{-j\frac{\pi}{2}[Mn^2+2(m_k^u-l_k)n]\right\}\\&=1+\exp\left\{-j\pi(m_k^u-l_k)\right\}.\end{aligned} \tag{64}$$

Likewise, if $|m_k^u-l_k|$ is odd, then $\mathcal{C}=0$, which leads to $I_k^u=0$; if $|m_k^u-l_k|$ is even, then $\mathcal{C}=2$ and I_k^u can be further simplified as

$$\begin{aligned}I_k^u&=2\sqrt{\frac{M}{2}}\exp\left\{j\frac{\pi}{4}\right\}\exp\left\{-j\frac{\pi}{2M}(m_k^u-l_k)^2\right\}\\&=2\sqrt{\frac{M}{2}}\mathcal{D},\end{aligned} \tag{65}$$

where $\mathcal{D}=\exp\left\{j\frac{\pi}{4}\right\}\exp\left\{-j\frac{\pi}{2M}(m_k^u-l_k)^2\right\}$.

REFERENCES

[1] U. Raza, P. Kulkarni and M. Sooriyabandara, "Low Power Wide Area Networks: An Overview," *IEEE Commun. Surveys Tuts.*, vol. 19, no. 2, pp. 855-873, 2rd Quart., 2017.

[2] J. P. Shanmuga Sundaram, W. Du and Z. Zhao, "A Survey on LoRa Networking: Research Problems, Current Solutions, and Open Issues," *IEEE Commun. Surveys Tuts.*, vol. 22, no. 1, pp. 371-388, 1st Quart., 2020.

[3] L. Vangelista, "Frequency Shift Chirp Modulation: The LoRa Modulation," *IEEE Signal Process. Lett.*, vol. 24, no. 12, pp. 1818-1821, Dec. 2017.

[4] M. Chiani and A. Elzanaty, "On the LoRa Modulation for IoT: Waveform Properties and Spectral Analysis," *IEEE Internet Things J.*, vol. 6, no. 5, pp. 8463-8470, Oct. 2019.

[5] T. Elshabrawy and J. Robert, "Closed-form approximation of LoRa modulation BER performance," *IEEE Commun. Lett.*, vol. 22, no. 9, pp. 1778-1781, Sep. 2018.

[6] R. Marini, K. Mikhaylov, G. Pasolini and C. Buratti, "Low-Power Wide-Area Networks: Comparison of LoRaWAN and NB-IoT Performance," *IEEE Internet Things J.*, vol. 9, no. 21, pp. 21051-21063, Nov. 2022.

[7] J. -M. Kang, "MIMO-LoRa for High-Data-Rate IoT: Concept and Precoding Design," *IEEE Internet Things J.*, vol. 9, no. 12, pp. 10368-10369, Jun. 2022.

[8] A. W. Azim, A. Bazzi, R. Shubair, and M. Chafii. *A Survey on Chirp Spread Spectrum-based Waveform Design for IoT.* [Online]. Available: https://arxiv.org/abs/2208.10274

[9] T. T. Nguyen, H. H. Nguyen, R. Barton and P. Grossetete, "Efficient Design of Chirp Spread Spectrum Modulation for Low-Power Wide-Area Networks," *IEEE Internet Things J.*, vol. 6, no. 6, pp. 9503-9515, Dec. 2019.

[10] R. Bomfin, M. Chafii and G. Fettweis, "A novel modulation for IoT: PSK-LoRa," in *Proc. IEEE Veh. Technol. Conf.*, Apr. 2019, pp. 1-5.

[11] T. Elshabrawy, P. Edward, M. Ashour and J. Robert, "On the Different Mathematical Realizations for the Digital Synthesis of LoRa-Based Modulation," in *25th European Wireless Conference*, pp. 1-6, 2019.

[12] I. Bizon Franco de Almeida, M. Chafii, A. Nimr and G. Fettweis, "Alternative Chirp Spread Spectrum Techniques for LPWANs," *IEEE Trans. Green Commun. Netw.*, vol. 5, no. 4, pp. 1846-1855, Dec. 2021.

[13] Q. Yu, D. He, Z. Lu and H. Wang, "SSK-Based PSK-LoRa Modulation for IoT Communications," *IEEE Open J. Commun. Soc.*, vol. 4, pp. 1487-1498, 2023.

[14] T. Elshabrawy and J. Robert, "Interleaved Chirp Spreading LoRa-Based Modulation," *IEEE Internet Things J.*, vol. 6, no. 2, pp. 3855-3863, Apr. 2019.

[15] M. Hanif and H. H. Nguyen, "Slope-shift keying LoRa-based modulation," *IEEE Internet Things J.*, vol. 8, no. 1, pp. 211-221, Jan., 2021.

[16] Y. Shi, W. Xu and L. Wang, "An Enhanced Interleaved Chirp Spreading LoRa Modulation Scheme for High Data Transmission," in *Proc. 2022 Wireless Telecommunications Symposium (WTS)*, 2022, pp. 1-6.

[17] A. Mondal, M. Hanif and H. H. Nguyen, "SSK-ICS LoRa: A LoRa-Based Modulation Scheme With Constant Envelope and Enhanced Data Rate," *IEEE Commun. Lett.*, vol. 26, no. 5, pp. 1185-1189, May 2022.

[18] I. B. F. de Almeida, M. Chafii, A. Nimr and G. Fettweis, "In-phase and quadrature chirp spread spectrum for IoT communications," in *Proc. IEEE Global Commun. Conf. (GLOBECOM)*, Taipei, Taiwan, Dec. 2020, pp. 1-6.

[19] S. An, H. Wang, Y. Sun, Z. Lu and Q. Yu, "Time Domain Multiplexed LoRa Modulation Waveform Design for IoT Communication," *IEEE Commun. Lett.*, vol. 26, no. 4, pp. 838-842, Apr. 2022.

[20] L. Vangelista and A. Cattapan, "A new LoRa-compatible modulation improving the LoRaWAN network level performance," in *Proc. IEEE Latin-Amer. Conf. Commun. (LATINCOM)*, 2019, pp. 1-6.

[21] Q. Yu, H. Wang, Z. Lu and S. An, "Group-Based CSS Modulation: A Novel Enhancement to LoRa Physical Layer," *IEEE Wireless Commun. Lett.*, vol. 11, no. 3, pp. 660-664, Mar. 2022.

[22] R. Hamdi and M. Qaraqe, "A Novel Index Modulation Based Chirp Spreading Modulation Scheme for Wireless Communications Systems," in *Proc. 2021 IEEE 94th Veh. Technol. Conf. (VTC2021-Fall)*, Norman, OK, USA, 2021, pp. 01-05.

[23] M. Hanif and H. H. Nguyen, "Frequency-Shift Chirp Spread Spectrum Communications With Index Modulation," *IEEE Internet Things J.*, vol. 8, no. 24, pp. 17611-17621, Dec. 2021.

[24] H. Ma, Y. Fang, G. Cai, G. Han and Y. Li, "A New Frequency-Bin-Index LoRa System for High-Data-Rate Transmission: Design and Performance Analysis," *IEEE Internet Things J.*, vol. 9, no. 14, pp. 12515-12528, Jul. 2022.

[25] A. W. Azim, J. L. G. Monsalve and M. Chafii, "Enhanced PSK-LoRa," *IEEE Wireless Commun. Lett.*, vol. 11, no. 3, pp. 612-616, Mar. 2022.

[26] A. W. Azim, A. Bazzi, R. Shubair and M. Chafii, "Dual-Mode Chirp Spread Spectrum Modulation," *IEEE Wireless Commun. Lett.*, vol. 11, no. 9, pp. 1995-1999, Sept. 2022.

[27] X. Yu, X. Cai, W. Xu, H. Sun and L. Wang, "Differential Phase Shift Keying-Aided Multi-Mode Chirp Spread Spectrum Modulation," *IEEE Wireless Commun. Lett.*, vol. 13, no. 2, pp. 298-302, Feb. 2024.

[28] G. Baruffa and L. Rugini, "Performance of LoRa-Based Schemes and Quadrature Chirp Index Modulation," *IEEE Internet Things J.*, vol. 9, no. 10, pp. 7759-7772, May 15, 2022.

[29] A. W. Azim, A. Bazzi, R. Bomfin, R. Shubair and M. Chafii, "Layered Chirp Spread Spectrum Modulations for LPWANs," *IEEE Trans. Commun.*, vol. 72, no. 3, pp. 1671-1687, Mar. 2024.

[30] Y. Bouazizi, F. Benkhelifa, H. ElSawy and J. A. McCann, "On the Scalability of Duty-Cycled LoRa Networks With Imperfect SF Orthogonality," *IEEE Wireless Commun. Lett.*, vol. 11, no. 11, pp. 2310-2314, Nov. 2022.

[31] A. Staikopoulos, V. Kanakaris and G. A. Papakostas, "Image Transmission via LoRa Networks – A Survey," in *Proc. IEEE Int. Conf. Image, Vis. Comput.*, Beijing, China, 2020, pp. 150-154.

[32] D. Magrin, M. Capuzzo, A. Zanella, L. Vangelista and M. Zorzi, "Performance Analysis of LoRaWAN in Industrial Scenarios," *IEEE Trans. Ind. Informat.*, vol. 17, no. 9, pp. 6241-6250, Sept. 2021.

[33] G. Baruffa, L. Rugini, V. Mecarelli, L. Germani and F. Frescura, "Coded LoRa performance in wireless channels," in *Proc. IEEE Annu. Int. Symp. Pers. Indoor Mobile Radio Commun. (PIMRC)*, Sep. 2019, pp. 1-6.

[34] O. Afisiadis, A. Burg and A. Balatsoukas-Stimming, "Coded LoRa frame error rate analysis," in *Proc. IEEE Int. Conf. Commun. (ICC)*, Jun. 2020, pp. 1-6.

[35] S. An, Z. Lu, H. Wang and Q. Yu, "A Turbo Coded LoRa-Index Modulation Scheme for IoT Communication," in *Proc. IEEE 21st Int. Conf. Commun. Technol.*, Tianjin, China, 2021, pp. 736-740.

[36] J. Bourduge, C. Poulliat, B. Gadat and J. F. Chouteau, "Bit interleaved chirp spread spectrum coded modulations with iterative decoding based on LDPC codes for coherent and non-coherent regimes," in *Proc. IEEE 33rd Annu. Int. Symp. Pers., Indoor Mobile Radio Commun. (PIMRC)*, Kyoto, Japan, 2022, pp. 968-974.

[37] Y. Guo and Z. Liu, "Time-Delay-Estimation-Liked Detection Algorithm for LoRa Signals Over Multipath Channels," *IEEE Wireless Commun. Lett.*, vol. 9, no. 7, pp. 1093-1096, Jul. 2020.

[38] U. Noreen, L. Clavier and A. Bounceur, "LoRa-like CSS-based PHY layer, Capture Effect and Serial Interference Cancellation," in *Proc. 24th Eur. Wireless Conf.*, 2018, pp. 1-6.

[39] A. Hoeller, R. D. Souza, O. L. Alcaraz López, H. Alves, M. de Noronha Neto and G. Brante, "Analysis and Performance Optimization of LoRa Networks With Time and Antenna Diversity," *IEEE Access*, vol. 6, pp. 32820-32829, 2018.

[40] L. -T. Tu, A. Bradai, Y. Pousset and A. I. Aravanis, "On the Spectral Efficiency of LoRa Networks: Performance Analysis, Trends and Optimal Points of Operation," *IEEE Trans. Commun.*, vol. 70, no. 4, pp. 2788-2804, Apr. 2022.

[41] O. Afisiadis, M. Cotting, A. Burg and A. Balatsoukas-Stimming, "On the Error Rate of the LoRa Modulation With Interference," *IEEE Trans. Wireless Commun.*, vol. 19, no. 2, pp. 1292-1304, Feb. 2020.

[42] D. Zorbas and X. Fafoutis, "Time-Slotted LoRa Networks: Design Considerations, Implementations, and Perspectives," *IEEE Internet Things Mag.*, vol. 4, no. 1, pp. 84-89, Mar. 2021.

[43] M. Xhonneux, J. Tapparel, A. Balatsoukas-Stimming, A. Burg and O. Afisiadis, "A Maximum-Likelihood-Based Two-User Receiver for LoRa Chirp Spread-Spectrum Modulation," *IEEE Internet Things J.*, vol. 9, no. 22, pp. 22993-23007, Nov. 2022.

[44] J. Tapparel, M. Xhonneux, D. Bol, J. Louveaux and A. Burg, "Enhancing the Reliability of Dense LoRaWAN Networks With Multi-User Receivers," *IEEE Open J. Commun. Soc.*, vol. 2, pp. 2725-2738, 2021.

[45] B. C. Berndt, K. S. Williams, and R. J. Evans. Gauss and Jacobi Sums. 1998.